

## ORIGINAL RESEARCH ARTICLE

# Neutrophil extracellular traps in gallbladder cancer: Mapping regulatory networks, identifying candidate targets, and characterizing pathway dysregulation

Jintao Liang<sup>1,2†</sup> , Yalun Liang<sup>1,2†</sup>, Yimao Wu<sup>1,3†</sup> , Shuai Ren<sup>4\*</sup> , and Meng-Yao Li<sup>1,5\*</sup> 

<sup>1</sup>Shanghai Cancer Institute, Renji Hospital, School of Medicine, Shanghai Jiao Tong University, Shanghai, China

<sup>2</sup>The First School of Clinical Medicine, Guangdong Medical University, Zhanjiang, Guangdong, China

<sup>3</sup>The Second School of Clinical Medicine, Guangdong Medical University, Dongguan, Guangdong, China

<sup>4</sup>Department of Radiology, Affiliated Hospital of Nanjing University of Chinese Medicine, Nanjing, Jiangsu, China

<sup>5</sup>Shanghai Key Laboratory of Cancer Systems Regulation and Clinical Translation, Shanghai Jiading District Central Hospital, Shanghai, China

*†These authors contributed equally to this work.*

### \*Corresponding authors:

Shuai Ren  
(shuair@njucm.edu.cn)  
Meng-Yao Li  
(limy@sioc.ac.cn)

**Citation:** Liang J, Liang Y, Wu Y, Ren S, Li M-Y. Neutrophil extracellular traps in gallbladder cancer: Mapping regulatory networks, identifying candidate targets, and characterizing pathway dysregulation. *Innov Med Omics*. 2026;3(2):025400052. doi: 10.36922/IMO025400052

**Received:** October 1, 2025

**Revised:** December 10, 2025

**Accepted:** December 24, 2025

**Published online:** February 27, 2026

**Copyright:** © 2026 Author(s). This is an Open-Access article distributed under the terms of the Creative Commons Attribution License, permitting distribution, and reproduction in any medium, provided the original work is properly cited.

**Publisher's Note:** AccScience Publishing remains neutral with regard to jurisdictional claims in published maps and institutional affiliations.

## Abstract

Gallbladder cancer (GBC) is an aggressive malignancy with limited therapeutic options. The role of neutrophil extracellular traps (NETs) in GBC remains unexplored. This study performed an integrated bioinformatics analysis using two Gene Expression Omnibus datasets (GSE138109 and GSE276931) to investigate NET-associated molecular mechanisms in GBC. After batch correction, differential expression analysis and weighted gene co-expression network analysis identified phenotype-associated modules. Intersection with high-confidence NET-related genes revealed 54 core genes linking NETs to GBC. Linear mixed model analysis highlighted significant downregulation of *ADAMTS1*, *GPX3*, and *MYH11* in tumor tissues. Pathway activity analysis showed the upregulation of cell-cycle pathways (E2F\_TARGETS and G2M\_CHECKPOINT) and the downregulation of inflammatory pathways (MYOGENESIS and TNFA\_SIGNALING\_VIA\_NFKB). These findings map a regulatory network through which NETs may influence GBC progression by disrupting extracellular matrix integrity and oxidative balance. The study provides a preliminary framework for mechanistic and therapeutic exploration, aligning with the need for molecularly informed strategies in advanced biliary tract cancer.

**Keywords:** Gallbladder cancer; Neutrophil extracellular traps; Bioinformatics analysis; *ADAMTS1*; *GPX3*; Pathway dysregulation; Precision oncology

## 1. Introduction

Gallbladder cancer (GBC) is the most common malignant tumor of the biliary tract, exhibiting unique global epidemiological characteristics with significant geographical

differences and gender imbalances.<sup>1</sup> According to the most recent statistics for 2025, the United States will document 12,610 new cases of GBC and adjacent bile duct cancer, of which GBC will constitute approximately 40%. The incidence in females surpasses that in males, with a male-to-female ratio of roughly 1:1.1.<sup>2</sup> In the global context, GBC typically manifests with subtle initial symptoms and undergoes swift progression, leading to the majority of patients being identified at advanced stages.<sup>3</sup> The global five-year survival rate stands at only 5%, while patients with early-stage disease who receive radical surgery can anticipate a five-year survival rate of 85–100%; those with advanced stages generally have a median survival of less than one year.<sup>4</sup> Given its considerable disease burden, GBC is increasingly recognized as a formidable global public health concern, particularly in areas with limited medical resources, such as the Andean region of South America and certain areas in sub-Saharan Africa.

In clinical practice, the “Expert Consensus on Conversion Therapy of Biliary Tract Cancer”<sup>5</sup> has significantly contributed to the standardization of management for biliary tract malignancies, including GBC. It particularly focuses on conversion therapy, defining the eligible patient population, such as those with initially unresectable GBC who may become resectable following systemic treatment. Moreover, it optimizes combination strategies of systemic therapy for conversion purposes, thereby providing new management directions for advanced GBC. However, there are still significant limitations. Radical surgery remains the only potentially curative intervention.<sup>6</sup> For patients with unresectable or metastatic cases, first-line chemotherapy has limited efficacy and is prone to acquired resistance, with extremely limited second-line options.<sup>7</sup> In addition, adverse events related to chemotherapy, the lack of standardized management for cancer-related fatigue, and surgical risks all exert negative influences on treatment compliance and quality of life.<sup>8,9</sup> Therefore, there is an immediate necessity to explore novel therapeutic strategies for GBC.

Neutrophil extracellular traps (NETs) are web-like structures released by activated neutrophils. These structures are primarily composed of deoxyribonucleic acid (DNA), histones, and various antimicrobial proteins.<sup>10</sup> Originally identified for their role in host antimicrobial defense, where they trap and eliminate pathogens, recent studies have underscored the critical regulatory role of NETs in malignancies.<sup>11</sup> In colorectal and pancreatic cancers, NETs accelerate disease progression by promoting tumor cell proliferation and invasion, inducing angiogenesis, and suppressing anti-tumor immune responses. Their expression levels are also strongly

correlated with poor patient prognosis.<sup>12</sup> Moreover, drugs that target NET formation or degradation have demonstrated tumor-inhibiting potential in animal models of certain cancers.<sup>13,14</sup> This suggests promising clinical translational value and positions NETs as a novel target for cancer therapy. However, research on NETs in GBC remains largely unexplored. The involvement of NETs in GBC pathogenesis, associations with clinicopathological features and prognosis, and impacts on treatment response and adverse events remain unelucidated.<sup>15</sup>

This study systematically examines the expression patterns and molecular mechanisms of NETs in GBC. Through integrated bioinformatics analyses, it delineates NET-associated regulatory networks and identifies candidate molecular targets linked to GBC pathogenesis. The findings address a gap in existing knowledge and establish a novel theoretical framework for future research into NETs in GBC. This work paves the way for subsequent investigations aimed at developing precise diagnostic markers and optimized therapeutic strategies. In line with established guidelines, this study aligns closely with the core principle of “standardized and individualized conversion therapy for biliary tract cancer,” as suggested in the “Expert Consensus on Conversion Therapy of Biliary Tract Cancer.”<sup>5</sup> Furthermore, it resonates with the consensus emphasis on exploring novel molecular targets to boost the efficacy of conversion therapy for biliary tract malignancies, providing practical support for advancements in GBC clinical management.

## 2. Materials and methods

### 2.1. Data download

The GBC-related gene expression datasets were downloaded from the Gene Expression Omnibus (GEO) database, including GSE138109 (platform: GPL11154) and GSE276931 (platform: GPL24676). GSE138109 contains 20 tumor tissue samples and 20 adjacent normal tissue samples from 20 GBC patients, while GSE276931 contains 7 tumor tissue samples and 5 adjacent normal tissue samples from 5 GBC patients. The two datasets were used for subsequent analysis.

### 2.2. Data preprocessing and batch effect correction

Initially, a  $\log_2$  transformation was applied to the gene expression data from two downloaded datasets (GSE138109 and GSE276931) in order to standardize the distribution of the data. The ComBat algorithm (implemented in the sva R package version 3.48.0) was subsequently utilized to correct for batch effects within the transformed data. Specifically, we employed parametric empirical Bayes adjustment (par.prior=TRUE), which assumes that batch effects follow

a normal distribution and is more powerful for small sample sizes compared to non-parametric alternatives. This parametric approach estimates location (mean) and scale (variance) parameters for each batch and shrinks batch effect estimates toward the overall mean using empirical Bayes, thereby achieving robust correction while preserving biological variation. This aimed to eradicate any systematic errors that may have arisen due to experimental batch differences between the two datasets. Principal component analysis (PCA) was then performed on the data, both pre- and post-batch effect correction, as a means of reducing dimensionality. The PCA was performed using the `prcomp()` function in R with parameters `center=TRUE` (to center variables to zero mean) and `scale=TRUE` (to standardize variables to unit variance) on the transposed expression matrix. PCA plots were generated to provide a visual representation of the increased consistency in the data following the removal of batch effects. To mitigate the risk of over-correction that could potentially remove true biological variation, we visually inspected the preservation of tumor-normal separation in post-correction PCA plots. The clear maintenance of biological grouping after correction (Figure 1) confirmed that batch adjustment did not eliminate genuine disease-related signals.

### 2.3. Screening and visualization of differentially expressed genes

Utilizing the consolidated dataset post-batch effect correction, pertinent statistical methodologies were employed using the `limma` package (version 3.56.2). A design matrix was constructed using `model.matrix()` with formula `~0 + factor(group)`, and differential expression was assessed using linear modeling (`lmFit`), contrast analysis (`makeContrasts: Treatment - Control`), and empirical Bayes moderation (`eBayes`). Results were extracted using `topTable()` with Benjamini-Hochberg false discovery rate (FDR) correction to identify differentially expressed genes (DEGs) between GBC tumor tissues and corresponding normal tissues. The selection criteria were established at  $p\text{-value} < 0.05$  and an FDR of  $< 0.25$ .

Given the relatively small sample size ( $n = 25$  patients) and the exploratory nature of this study, which investigates the novel NET-GBC association for the first time, we adopted a more lenient FDR threshold (0.25 instead of the conventional 0.05) to minimize false negatives and capture potentially relevant genes that warrant further validation in larger cohorts.

To illustrate the distribution of gene expression disparities, a volcano plot was crafted using the identified DEGs. The volcano plot features color-coded genes: downregulated (green, #0dffa5), not significant (gray,

#808080), and upregulated (purple, #962ae4), with threshold lines at absolute  $\log_2$  fold change ( $|\log_2FC| = 1$ ) and FDR = 0.25. The top 20 most significant genes were labeled using the `ggrepel` package (version 0.9.4) to avoid overlapping. Furthermore, the most significant 200 DEGs, as ranked by  $|\log_2FC|$  values, were chosen to generate a heatmap. This heatmap elucidates the variations in expression patterns of these genes across samples, differentiated by the data source: GSE138109, denoted in green, and GSE276931 in purple.

### 2.4. Weighted gene co-expression network analysis

The weighted gene co-expression network analysis (WGCNA) method was employed to construct a co-expression network, encompassing all genes within the integrated dataset. The genes were clustered into distinct modules based on the similarity of their expression patterns, yielding 18 modules (ME0, ME1, ..., ME16, and a grey module). The grey module was subsequently excluded from further analyses due to its ambiguous biological significance. The correlation between each module and the phenotype was calculated, designating "tumor tissue" and "normal tissue" as phenotypic traits. The Pearson correlation coefficient was utilized to measure the strength of the correlation, ranging from  $-1$  to  $1$ , where positive values denote a positive correlation. The  $p$ -value was employed to evaluate the statistical significance of the correlation. A heatmap representing the module-phenotype correlation was plotted, and key modules exhibiting an absolute Pearson correlation coefficient greater than 0.5 and a  $p$ -value less than 0.05 were identified.

### 2.5. Acquisition of neutrophil extracellular trap-related genes and intersection analysis

Genes associated with NETs were sourced from the GeneCards database. From these, genes that ranked in the top 25% in terms of relevance score were chosen to comprise the high-quality NET-related gene set, based on their pertinence to NETs. An intersection analysis was conducted among three gene sets: the top 200 DEGs ranked by  $\log_2FC$  values, the genes identified from key modules via WGCNA (ME2, ME4, ME10, and ME12), and the aforementioned high-quality NET-related genes. Genes common to all three sets were deemed core genes implicated in both NET regulation and GBC progression.

### 2.6. Visualization of expression differences in intersection genes

Two distinct visualizations were created for the core intersection genes acquired from the preceding step. Prior to visualization, gene expression values were z-score-normalized across samples (mean = 0, standard deviation

= 1) to enable comparison across genes with different expression scales and to highlight relative expression patterns.

Firstly, a heatmap was designed to depict the expression distribution of these genes within both GBC tumor tissues and their corresponding normal tissues, thereby illustrating the variances in overall expression patterns. Secondly, a boxplot was employed to visually represent the statistical differences in these genes' expression levels across the two tissue types. This approach emphasizes the magnitude of expression variations.

Statistical significance of expression differences between tumor and normal tissues in boxplots was assessed using the Wilcoxon rank-sum test (Mann-Whitney U test), a non-parametric test appropriate for comparing two independent groups. A  $p$ -value < 0.05 was considered statistically significant.

## 2.7. Linear mixed model analysis of core intersection genes

The core intersection genes were subjected to a linear mixed model (LMM) analysis, using normal tissues as the reference group. This model incorporated baseline differences among patients, including individual variations in baseline gene expression levels and experimental detection errors. For each gene, three critical metrics were computed: coefficient,  $p$ -value, and FDR. The coefficient value denotes the average expression difference of a gene between tumor and normal tissues, after adjusting for inter-patient baseline differences. Genes with the top 25% absolute coefficient values, and satisfying the criteria of  $p$ -value < 0.05 and FDR < 0.25, were identified to determine the core genes with the most significant downregulation in GBC.

The LMM was implemented using lme4 (version 1.1-35.1) with Equation (1):

$$Expression \approx Group + (1|Patient) \quad (1)$$

where *Expression* is the gene expression level, *Group* is the tissue type (tumor vs. normal) as a fixed effect, and (1|Patient) is a random intercept accounting for patient-specific variability and paired samples. Statistical significance was assessed using lmerTest (version 3.1-3) with Satterthwaite's approximation. Genes with absolute coefficient values in the top 25%,  $p$  < 0.05, and FDR < 0.25 were selected as key differentially regulated genes.

## 2.8. Pathway activity analysis and linear mixed model screening of key pathways

The single-sample Gene Set Enrichment Analysis (ssGSEA) was employed to assess the activity levels of pathways

within each sample. The h.all.v2025.1.Hs.symbols.gmt database, which encompasses 50 prevalent pathways and their associated genes, served as a reference. This reference database was utilized in conjunction with the merged gene expression matrix, which was then input into the ssGSEA algorithm. Consequently, an activity score for each pathway within each sample was computed, yielding a pathway activity score matrix. Subsequent LMM analysis, using normal tissues as a reference group, facilitated the identification of pathways exhibiting significant activity disparities in GBC. The screening criteria were established at the top 25% absolute coefficient values, with a  $p$ -value < 0.05, and FDR < 0.25, pinpointing key pathways that were either upregulated or downregulated in GBC.

## 2.9. Statistical analysis

All data analyses were conducted utilizing R language (Version 4.4.2) with the following key packages: limma (version 3.56.2) for differential expression analysis, WGCNA (version 1.72-1) for WGCNA, sva (version 3.48.0) for ComBat batch correction, lme4 (version 1.1-35.1) for LMMs, lmerTest (version 3.1-3) for model significance testing, GSVA (version 1.48.0) for ssGSEA pathway activity scoring, ggplot2 (version 3.4.4) for visualization, and ggrepel (version 0.9.4) for gene label annotation.

A  $p$ -value of less than 0.05 and an FDR of less than 0.25 were deemed to signify statistically significant differences. All statistical tests were two-sided unless otherwise specified.

## 3. Results

### 3.1. Data acquisition and batch effect correction

Two gene expression datasets associated with GBC, namely GSE138109 and GSE276931, were downloaded. The GSE138109 dataset comprised 20 tumor samples and 20 adjacent normal samples collected from 20 patients. Likewise, the GSE276931 dataset incorporated seven tumor samples and five adjacent normal samples obtained from five patients. Subsequent to log2 transformation and ComBat batch-effect correction, the PCA plot (Figure 1) revealed that prior to the correction of batch effects, there was a significant separation between the samples from the two datasets in the principal component space. However, post correction, the samples exhibited a more compact clustering, effectively eliminating the batch effects and significantly enhancing data consistency. Consequently, the merged dataset was deemed suitable for subsequent analyses.

### 3.2. Differentially expressed gene screening

Utilizing  $p$ -value < 0.05 and FDR < 0.25 as selection

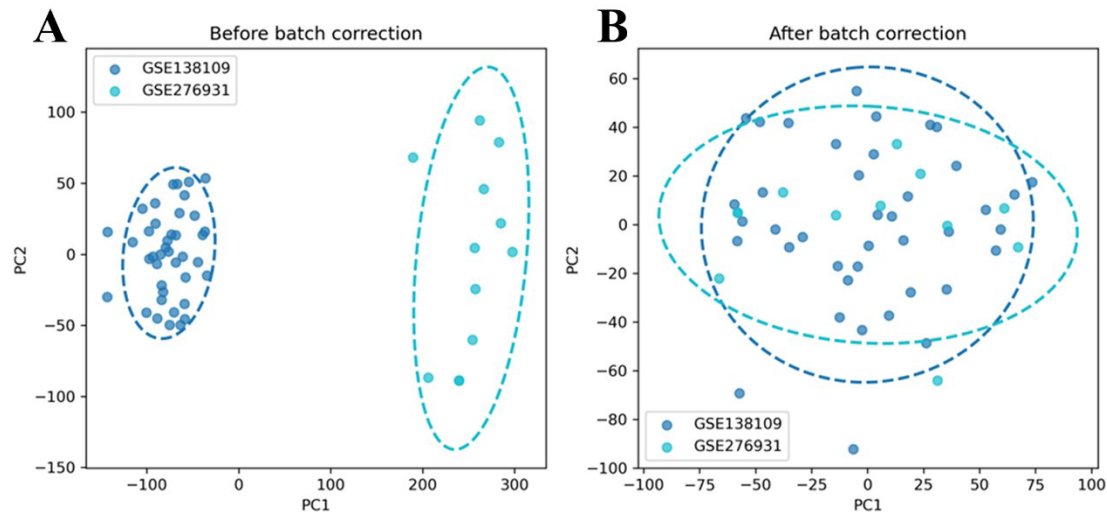


**Figure 1.** Principal component analysis (PCA) plots of data (A) before and (B) after batch effect correction. PCA visualization showing sample distribution along principal component axes (PC1 and PC2) before and after batch effect correction. (A) Samples show clear separation by dataset origin (GSE138109 vs. GSE276931) before correction. (B) Samples exhibit improved clustering by tissue type (tumor vs. normal) after ComBat correction, with reduced batch-related variation. PC1 and PC2 capture the two largest sources of variation in the data.

parameters, a total of 575 DEGs, including 169 upregulated and 406 downregulated genes, were identified between GBC tumor tissues and adjacent normal tissues from the integrated dataset. This identification was visualized through a volcano plot (Figure 2), which distinctly showcased the distribution of DEGs. Genes that were significantly upregulated or downregulated were highlighted, providing an intuitive representation of the gene expression disparity between the two tissue types. Moreover, the top 200 DEGs, based on logFC values, were employed to construct a heatmap (Figure A1). The findings revealed pronounced differences in gene expression patterns between tumor and normal tissues. Notably, samples from diverse datasets (with GSE138109 denoted in green and GSE276931 in purple) exhibited consistent gene expression trends, thereby affirming the dependability of the selected DEGs.

Quantitative validation through sample correlation analysis and hierarchical clustering confirmed that samples clustered primarily by tissue type rather than dataset origin, thereby affirming successful batch correction and the dependability of the selected DEGs for subsequent analyses.

### 3.3. Module–phenotype correlation analysis

Utilizing WGCNA, the genes within the consolidated dataset were categorized into 18 distinct modules, denoted as ME0–ME16 and a grey module. The grey module was subsequently omitted from further analyses due to its perceived lack of biological relevance. A detailed

examination of the module–phenotype correlation heatmap (Figure 3) unveiled significant disparities in both the Pearson correlation coefficients and the associated *p*-values across various modules when juxtaposed with the “tumor/normal” phenotype. Notably, modules ME2, ME4, ME10, and ME12 exhibited an absolute Pearson correlation coefficient exceeding 0.5, coupled with a *p*-value less than 0.05, signifying a robust correlation with tumor–normal status. Consequently, these four modules were designated as key modules.

### 3.4. Functional enrichment analysis

The ME2 module (1,911 genes) was predominantly enriched in extracellular matrix (ECM) organization and cell–matrix adhesion processes. Gene Ontology (GO) analysis revealed the highest enrichment for ECM-related biological processes (“extracellular matrix organization”), cellular components (“collagen-containing ECM”), and molecular functions (“ECM structural constituent” and “integrin binding”),<sup>16,17</sup> along with cell movement processes including “chemotaxis” and “leukocyte migration.” Kyoto Encyclopedia of Genes and Genomes (KEGG) pathway analysis identified “integrin signaling” and “focal adhesion” as the most significantly enriched pathways. This functional profile strongly indicates ME2’s participation in tumor microenvironment remodeling, a hallmark of cancer progression,<sup>18</sup> with the ECM-related enrichment aligning with the known role of NETs in promoting ECM degradation through proteolytic enzyme release.<sup>19,20</sup> The presence of *ADAMTS1*, a key downregulated gene



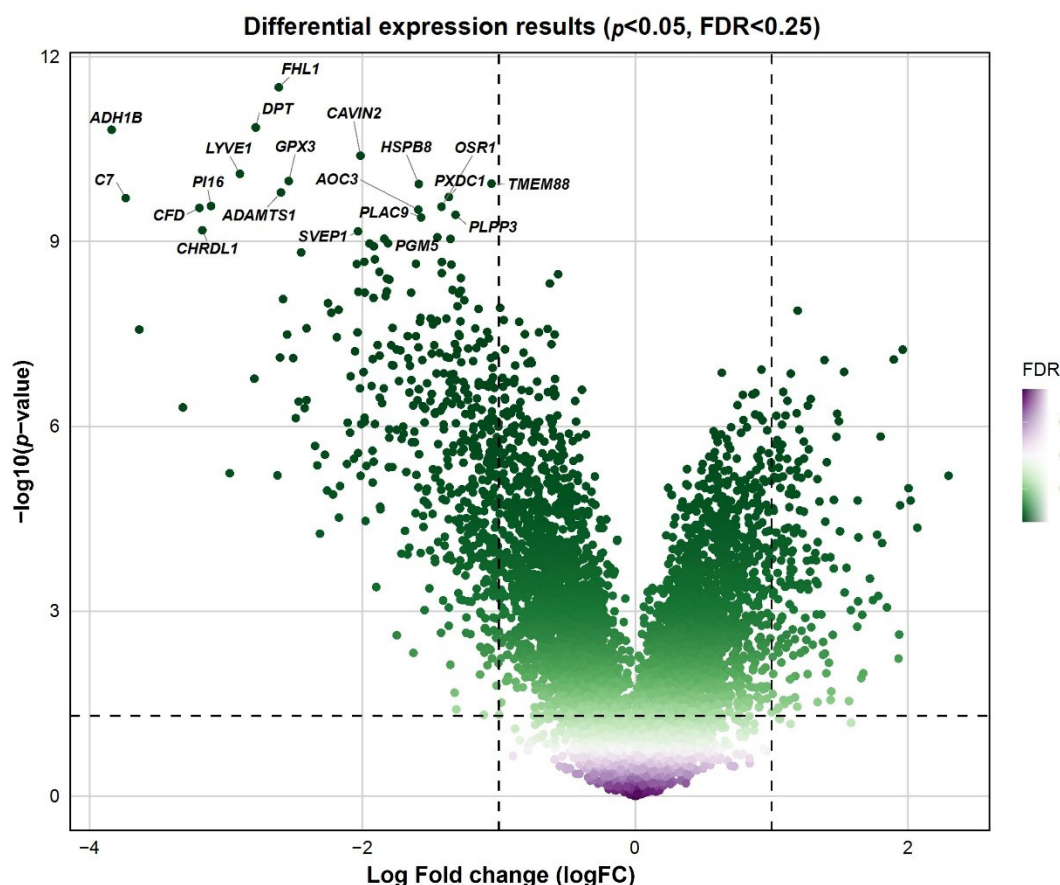


**Figure 2.** Volcano plot of differentially expressed genes (DEGs). Plot displaying the distribution of DEGs between GBC tumor and adjacent normal tissues ( $p < 0.05$ , FDR  $< 0.25$ ). Genes are color-coded: upregulated in tumor (purple), downregulated in tumor (green), and not significant (gray). Abbreviation: FDR: False discovery rate.

in our core set, is particularly relevant, as a disintegrin and metalloproteinase with thrombospondin motifs (ADAMTS) family proteins are critical ECM proteinases whose dysregulation may create an environment conducive to NET-mediated tumor invasion.<sup>21</sup>

The ME4 module (454 genes) exhibited strong enrichment in cell cycle-related processes, with GO analysis revealing “chromosome segregation” as the most significant term, along with enrichment in “chromosomal region” (cellular component) and “chromatin structural constituent” (molecular function). KEGG pathway analysis identified “cell cycle” as the most enriched pathway,<sup>22</sup> with the remarkable finding that “neutrophil extracellular trap formation” appears as the third most enriched pathway, providing direct molecular evidence linking NET biology with cancer cell proliferation.<sup>23–25</sup> This enrichment pattern is consistent with our pathway activity analysis showing upregulation of E2F targets and G2M checkpoint pathways in GBC tissues, suggesting that NETs may not only modify the tumor microenvironment but also directly

influence cancer cell cycle machinery. The coordinated upregulation of cell cycle processes in the context of NET-associated inflammation potentially reflects the loss of normal checkpoint control, contributing to the aggressive proliferative phenotype of GBC.

The ME10 module (86 genes) was enriched in muscle-related and cytoskeletal processes, with GO analysis showing the highest enrichment for “muscle system process,” “contractile fiber,” and “muscle structural constituent” (molecular function). KEGG pathway analysis identified “actin cytoskeleton in muscle cells” and “vascular smooth muscle contraction” as primary enriched pathways. In the cancer biology context, these terms indicate involvement in cytoskeletal dynamics, cellular contractile force, and cell motility. The presence of *MYH11* (myosin heavy chain 11), a core downregulated gene essential for smooth muscle contraction and cellular contractile force, is particularly relevant, as its downregulation may reduce cellular mechanical tension and adhesion strength, facilitating tumor cell detachment and invasion. The enrichment of

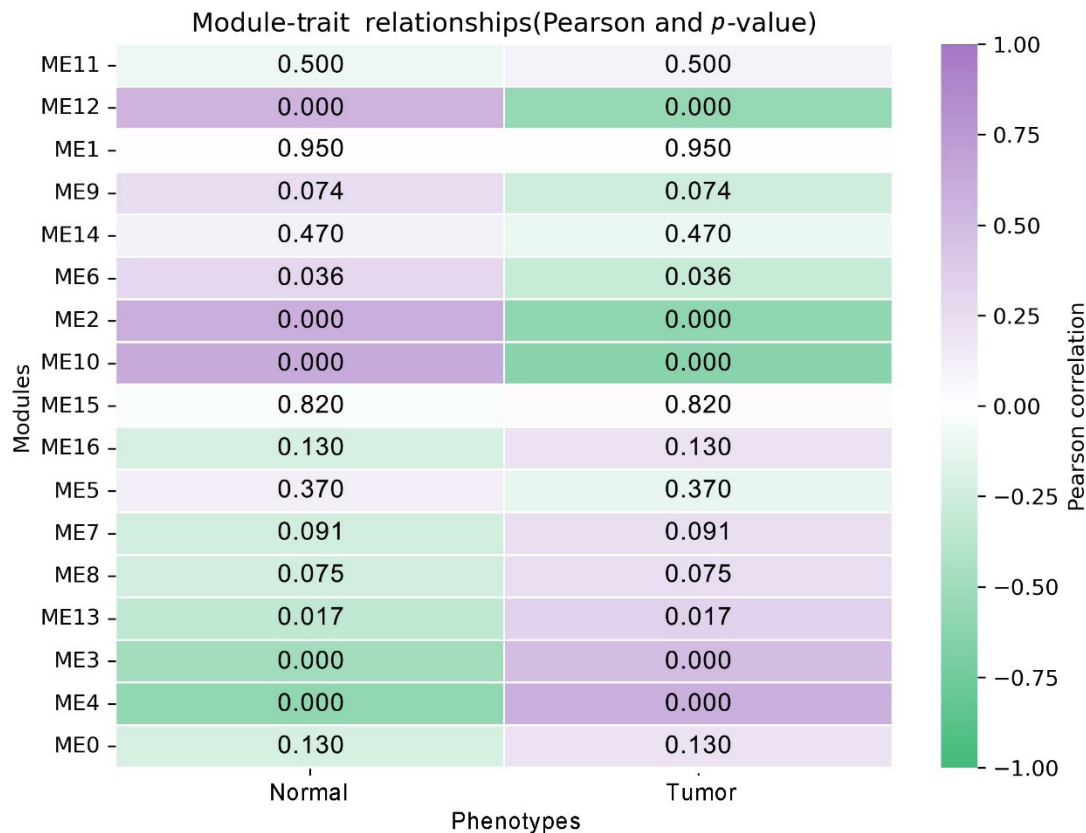


**Figure 3.** Module–phenotype correlation heatmap. Heatmap of Pearson correlation coefficients and *p*-values between weighted gene co-expression network analysis modules and “tumor/normal” phenotype.

stress fiber components suggests ME10 genes regulate actomyosin contractility, critical for cancer cell migration and invasion,<sup>26</sup> with NETs potentially altering tumor cell cytoskeletal dynamics through released proteases and histones, leading to ME10 module dysregulation.<sup>27</sup>

The ME12 module (75 genes) was enriched in lipid metabolism-related processes, with GO biological process analysis revealing significant enrichment of “lipid storage” and “lipid catabolic process,” along with cellular component enrichment in “lipid droplet” and membrane microdomains, including “caveola” and “membrane raft.” This lipid metabolism enrichment is particularly relevant to GBC, given the organ’s central role in bile storage and lipid digestion,<sup>28</sup> with the balance between lipid storage and catabolism being crucial for cellular energy homeostasis and membrane biosynthesis in rapidly proliferating cancer cells. The presence of *GPX3* (glutathione peroxidase 3), a core downregulated gene and key antioxidant enzyme, is significant in this module, as NETs induce oxidative stress through reactive oxygen species (ROS) and myeloperoxidase release,<sup>29</sup> and *GPX3* downregulation in the context of NET-associated oxidative stress would

impair cellular antioxidant defense, potentially leading to oxidative damage accumulation, lipid peroxidation, and metabolic dysregulation. ME12 genes also potentially regulate membrane lipid organization and signaling platform formation that could be disrupted by NET-induced oxidative stress.

Functional enrichment analysis of the four key modules revealed a multidimensional regulatory network in NET-associated GBC pathogenesis (Figure 4), with each module representing a distinct biological dimension: ME2 (tumor microenvironment) coordinates ECM remodeling and cell-matrix interactions through integrin signaling and focal adhesion pathways, with dynamic ECM remodeling involving complex interactions among ECM components, immune cells, and the vascular system;<sup>30,31</sup> ME4 (proliferation) directly links NET biology to cell cycle control through co-enrichment of “neutrophil extracellular trap formation” and “cell cycle” pathways, demonstrating that NETs not only modify the tumor microenvironment but also directly influence cancer cell proliferation;<sup>32</sup> ME10 (invasion and motility) regulates cytoskeletal dynamics and cellular contractility with *MYH11* downregulation

potentially facilitating tumor cell dissemination; and ME12 (metabolic reprogramming) reflects lipid metabolism disruption with *GPX3* downregulation, creating a vicious cycle of metabolic dysregulation and oxidative damage.

These four modules represent interconnected nodes in a complex regulatory network, where ECM remodeling (ME2) provides structural support for cell proliferation (ME4) and creates channels for cell migration (ME10), while metabolic reprogramming (ME12) supplies the energy and building blocks required for these processes. NETs are positioned at the inflammation–cancer interface, acting as central coordinators orchestrating the synchronized dysregulation of all four modules,<sup>33,34</sup> thereby simultaneously driving multiple hallmarks of GBC progression.<sup>35</sup>

### 3.5. Core intersection gene screening

Genes associated with NETs were extracted from the GeneCard database, with only the top 25% of relevant genes (balances stringency with sensitivity) being selected for further analysis. We conducted an intersection analysis among the top 200 DEGs determined by logFC, the genes from four key modules identified by WGCNA (ME2, ME4, ME10, ME12), and the highly relevant NET-associated genes. This process yielded 54 intersection genes (Figure 5), which are essentially core genes involved in both the

regulation of NETs and the pathological progression of GBC. These genes represent promising targets for future research.

### 3.6. Heatmap analysis for 54 intersection genes

A heatmap illustrating the expression of the 54 intersection genes in both GBC tumor and adjacent normal tissues was generated (Figure 6). The distinct expression distribution patterns between the two tissue types were vividly displayed. Genes that were expressed more highly in normal tissues were represented by one color gradient, while those with increased expression in tumor tissues were depicted by another, effectively highlighting the overall disparities in gene expression profiles between the two groups.

### 3.7. Boxplot analysis for 54 intersection genes

A boxplot (Figure A2) was utilized to further scrutinize the expression differences of the 54 intersection genes between GBC tumor tissues and adjacent normal tissues. The results demonstrated that, in comparison to the heatmap, the boxplot provided a more distinct illustration of the statistical differences in gene expression levels between the two tissue types. The median, quartiles, and range of gene expression values in each group were vividly displayed, thereby affirming that the 54 intersection genes exhibited significantly different expression levels in tumor and normal tissues.

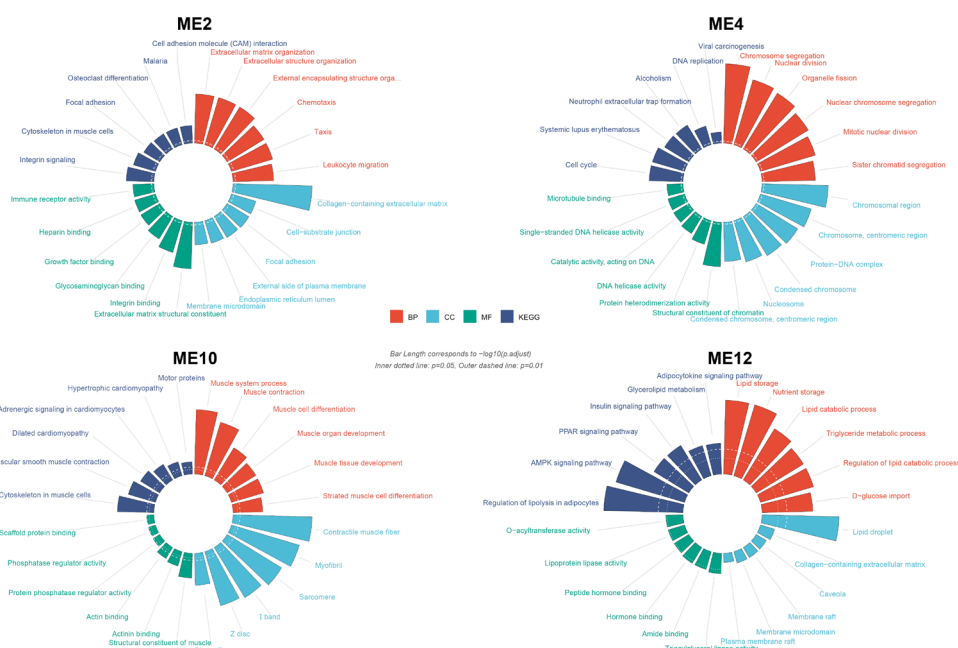


**Figure 4.** Diagram of enrichment analysis showing the enrichment results of key modules (ME2, ME4, ME10, and ME12)  
Abbreviations: BP: Biological process; CC: Cellular component; MF: Molecular function; KEGG: Kyoto Encyclopedia of Genes and Genomes.



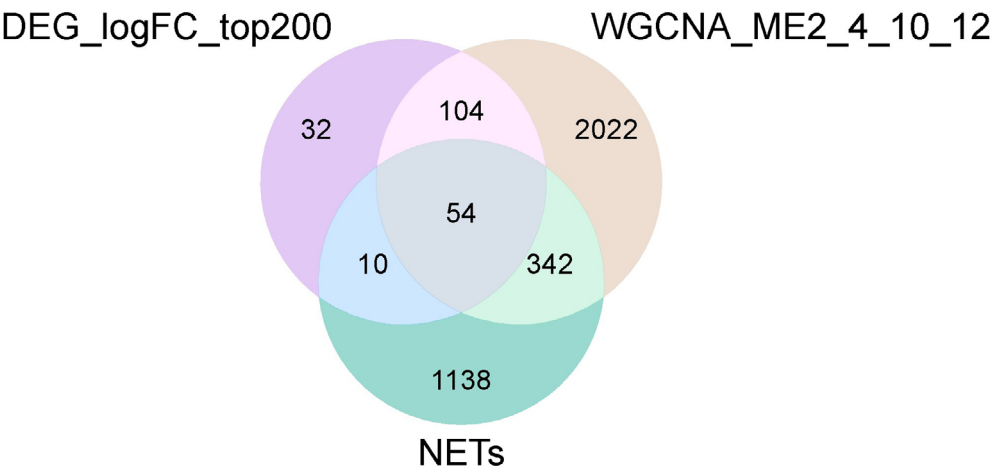


**Figure 5.** Venn diagram of core intersection genes. Venn diagram showing the overlap (54 intersection genes) among the top 200 differentially expressed genes (DEGs) ranked by  $|\log_2FC|$ , weighted gene co-expression network analysis (WGCNA) key module genes, and high-quality neutrophil extracellular trap (NET)-related genes.

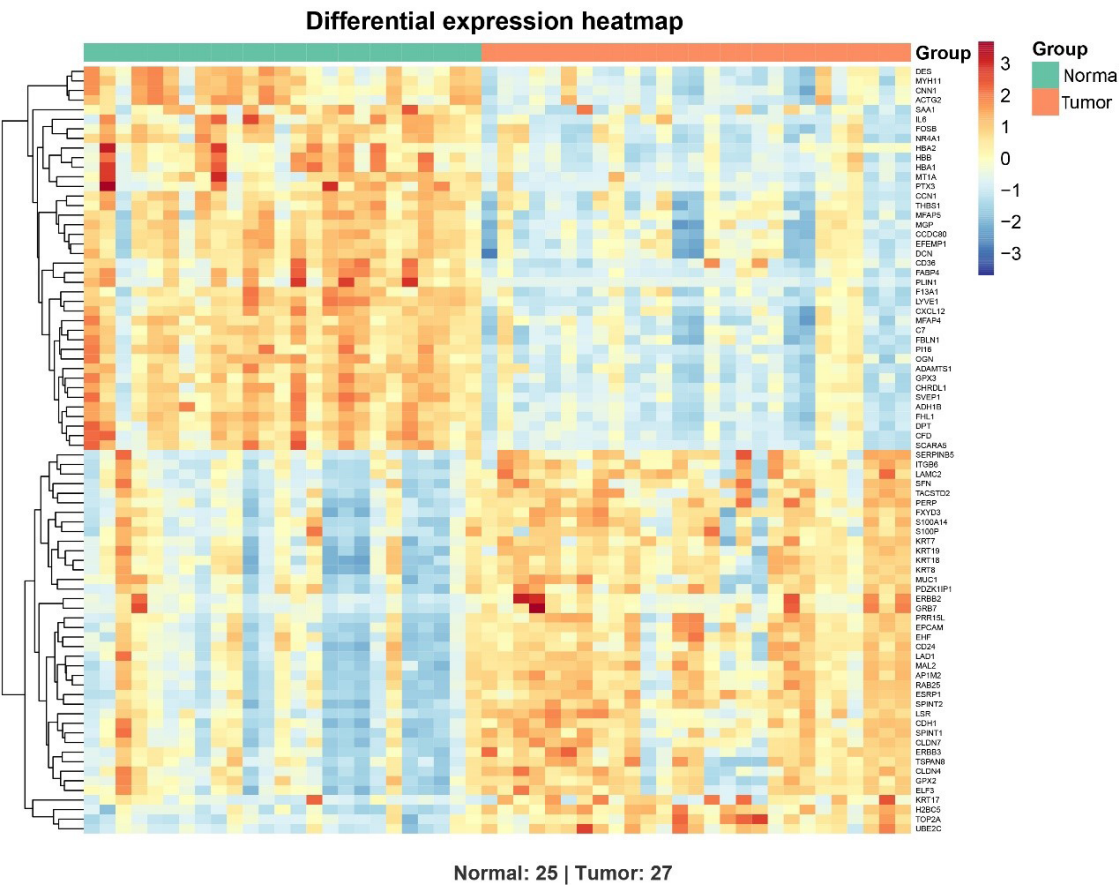


**Figure 6.** Heatmap displaying expression distribution of 54 core genes in gallbladder cancer tumor and adjacent normal tissues

### 3.8. Linear mixed model analysis for core intersection genes

The 54 intersection genes were subjected to LMM analysis, utilizing normal tissues as the reference group. Genes in the top 25% absolute coefficient values with a  $p$ -value < 0.05 and FDR < 0.25 were selected and visualized (Figure 7). Notably, genes such as *ADAMTS1\_ME2*, *GPX3\_ME2*, and *MYH11\_ME10* exhibited the most significant downregulation in GBC tumor tissues. Specifically, *ADAMTS1\_ME2* demonstrated a  $p$ -value of  $1.01 \times 10^{-10}$  and an FDR of  $2.74 \times 10^{-9}$ , while *GPX3\_ME2* recorded an exceptionally low  $p$ -value of  $6.61 \times 10^{-11}$  and an FDR of  $2.74 \times 10^{-9}$ . These results suggest that these genes may play a pivotal inhibitory role in the initiation and progression of GBC.

### 3.9. Pathway activity analysis and key pathway screening

The ssGSEA was employed to compute the activity score for each of the 50 prevalent pathways in every sample, thereby generating a pathway activity score matrix. Utilizing this matrix, an LMM analysis was performed, designating

normal tissues as the reference group. Pathways that exhibited the top 25% absolute coefficient values, with a  $p$ -value < 0.05 and FDR < 0.25, were meticulously selected (Figure 8). It is imperative to highlight that two specific pathways, namely *HALLMARK\_E2F\_TARGETS* ( $p = 4.34 \times 10^{-7}$ ) and *HALLMARK\_G2M\_CHECKPOINT* ( $p = 6.74 \times 10^{-7}$ , FDR =  $4.76 \times 10^{-6}$ ), manifested augmented activity in GBC tumor tissues. Conversely, the majority of other pathways, including *HALLMARK\_MYOGENESIS* ( $p = 4.38 \times 10^{-9}$ , FDR =  $2.19 \times 10^{-7}$ ) and *HALLMARK\_TNFA\_SIGNALING\_VIA\_NFKB* ( $p = 3.53 \times 10^{-7}$ , FDR =  $3.53 \times 10^{-6}$ ), demonstrated a significant diminution in activity within tumor tissues. It is thus inferred that these pathways potentially contribute to the pathological mechanism of GBC through the regulation of NET-associated genes.

## 4. Discussion

In this study, we conducted an analysis of the GSE138109 and GSE276931 datasets, obtained from the GEO database. Following batch effect correction, we screened for DEGs between GBC tissues and normal tissues. Utilizing WGCNA, we identified four key modules that exhibited

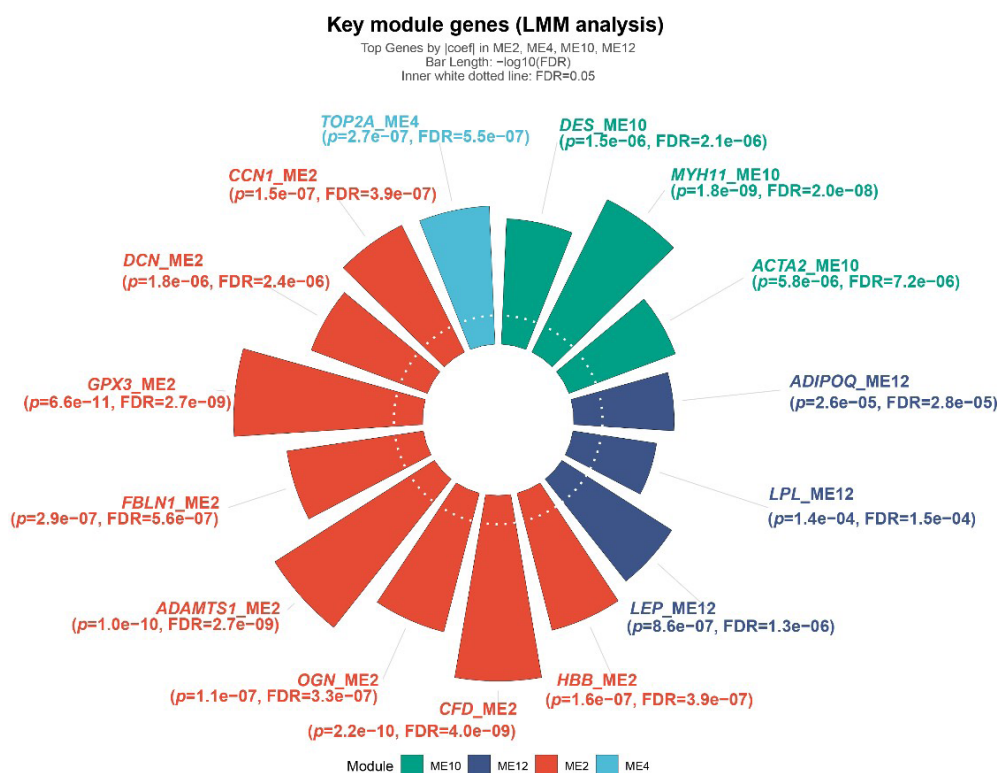


**Figure 7.** Results of linear mixed model (LMM) analysis for 54 intersection genes. Visualization of genes with top 25% absolute coefficient values ( $p < 0.05$ , FDR < 0.25), highlighting significantly downregulated genes (e.g., *ADAMTS1\_ME2* and *GPX3\_ME2*).

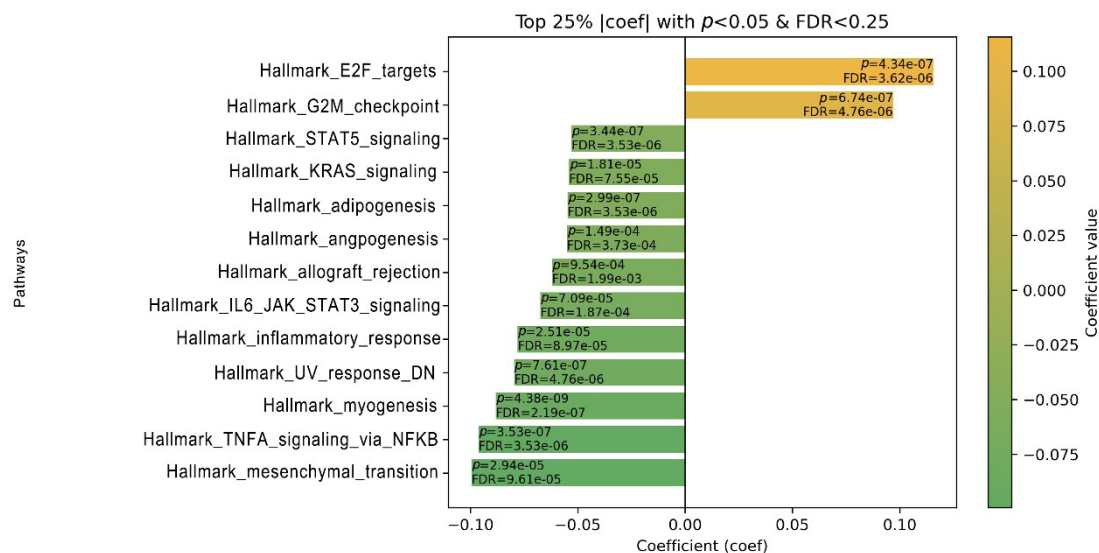


**Figure 8.** Results of linear mixed model analysis for pathway activity. Visualization of key pathways (top 25% absolute coefficient values,  $p < 0.05$ ,  $FDR < 0.25$ ), showing upregulated (e.g., *G2M\_CHECKPOINT*) and downregulated pathways.

a strong association with the GBC phenotype. Upon intersecting these modules with high-quality NET-related genes, we derived a set of 54 core genes. Subsequent LMM analysis revealed significant downregulation of genes such as *ADAMTS1*, *GPX3*, and *MYH11* in GBC. Furthermore, ssGSEA coupled with LMM analysis demonstrated an increase in the activities of the *E2F\_TARGETS* and *G2M\_CHECKPOINT* pathways in GBC, while revealing a decrease in the activities of the *MYOGENESIS* and *TNFA\_SIGNALING\_VIA\_NFKB* pathways.

#### 4.1. Association between neutrophil extracellular traps and gallbladder cancer core genes and evidence from existing studies

Existing research has unequivocally established that NETs expedite the progression of malignant tumors, such as colorectal and pancreatic cancers, by fostering tumor cell proliferation and invasion, stimulating angiogenesis, and impeding anti-tumor immune responses.<sup>36</sup> However, their regulatory function and molecular targets in GBC remain undefined. This study pioneers the exploration of 54 core genes implicated in both NET regulation and GBC progression, thereby providing crucial molecular insights into the relationship between the two. Mechanistically, NET formation is contingent on neutrophil activation, oxidative stress surges, and inflammatory response activation.<sup>37</sup> The core genes identified in this study are significantly enriched in these biological processes, indicating that NETs may contribute to the pathological process of GBC by modulating these genes. For example, *ADAMTS1*, a member of the metalloproteinase family,

has been demonstrated in prior studies to inhibit tumor invasion and metastasis by degrading the ECM in liver and breast cancer.<sup>38</sup> This study revealed that *ADAMTS1* is significantly downregulated in GBC. In conjunction with the ability of NETs to degrade ECM components such as collagen,<sup>39</sup> it is proposed that NETs may further compromise the integrity of the ECM barrier by inhibiting *ADAMTS1* expression. This effectively removes constraints on GBC cell invasion. This hypothesis aligns closely with the established mechanism by which NETs promote tumor metastasis.

As a key member of the glutathione peroxidase family, *GPX3* functions to scavenge intracellular ROS, thereby maintaining a balance in oxidative stress.<sup>40</sup> During the formation of NETs, a substantial quantity of ROS is released via the nicotinamide adenine dinucleotide phosphate (reduced form) (NADPH) oxidase pathway.<sup>41</sup> The observed downregulation of *GPX3* in this study may be linked to this NET-mediated accumulation of ROS. Excessive ROS can cause DNA damage and activate oncogenic signaling pathways, such as mitogen-activated protein kinase (MAPK),<sup>42</sup> ultimately creating a microenvironment that supports the malignant proliferation of GBC cells.<sup>43</sup> This hypothesis is further corroborated by existing research indicating that NETs promote tumor progression via ROS accumulation, as evidenced in studies on lung<sup>44</sup> and gastric cancers.<sup>45</sup>

#### 4.2. Biological significance of key pathway changes and clinical implications

The disparities in pathway activity discerned in this

study elucidate the potential molecular mechanism by which NETs modulate GBC, offering insights for clinical intervention strategies. Notably, the E2F\_TARGETS and G2M\_CHECKPOINT pathways exhibit significantly heightened activities in GBC. These pivotal pathways oversee the G1/S phase transition and G2/M phase checkpoint of the cell cycle,<sup>46,47</sup> respectively, and are fundamental to the unrestrained proliferation of tumor cells.<sup>48,49</sup> Previous research has indicated that histones, such as H3cit, liberated by NETs, can amplify the expression of cell cycle proteins, including cyclin D1 and cyclin-dependent kinase 4 (CDK4), through the activation of the phosphatidylinositol 3-kinase (PI3K)/Akt pathway.<sup>50,51</sup> The findings of this study indicate that NETs may further accelerate cell-cycle progression in GBC cells and shorten the cell cycle by engaging the E2F\_TARGETS and G2M\_CHECKPOINT pathways.

This study presents direct pathway-level evidence supporting the hypothesis that NETs promote GBC proliferation. It also suggests that targeting the MYOGENESIS (myogenesis) and TNFA\_SIGNALING\_VIA\_NFKB (tumor necrosis factor- $\alpha$  [TNF- $\alpha$ ]/nuclear factor-kappa B [NF- $\kappa$ B]) pathways could undermine the pro-tumor effect of NETs.<sup>52</sup> The reduced activity of these pathways is indicative of the unique GBC microenvironment. Notably, the TNF- $\alpha$ /NF- $\kappa$ B pathway serves as a critical nexus between inflammation and tumors.<sup>53,54</sup> Previous research has established that NETs can activate the NF- $\kappa$ B pathway by releasing neutrophil elastase, thereby promoting the secretion of interleukin (IL)-6 and TNF- $\alpha$  in colorectal cancer.<sup>55,56</sup> However, this pathway shows downregulation in GBC in the present study. This may be attributed to an imbalance in the synergistic relationship between NETs and other inflammatory factors (e.g., IL-1 $\beta$  and IL-8) within the GBC microenvironment. This aligns with the proposition in several studies that the regulation of the NF- $\kappa$ B pathway by NETs is tumor-specific.<sup>57,58</sup> Additionally, it hints at the possibility of a distinct mechanism of NETs in GBC, warranting further experimental validation. From a clinical translation perspective, the combined application of E2F\_TARGETS pathway inhibitors (e.g., retinoblastoma 1 [RB1] agonists) and NETs formation inhibitors (e.g., peptidylarginine deiminase 4 [PAD4] enzyme inhibitors) could potentially constitute a novel therapeutic strategy for GBC.<sup>59</sup> This is particularly relevant for patients exhibiting high NET expression and the activated E2F\_TARGETS pathway.

### 4.3. Study limitations and future directions

This study presents three significant limitations that necessitate consideration in future research endeavors. Firstly, all the data utilized in this study were extracted

from public GEO databases, consisting of a modest sample size of 25 patients in total. Furthermore, there was an absence of correlation analysis between clinicopathological information, such as tumor stage, lymph node metastasis status, and patient prognosis, and the expression levels of NETs. This gap in analysis makes it challenging to elucidate the relationship between core genes, pathways, NETs, and GBC clinical outcomes, potentially affecting the generalizability and clinical applicability of the results. Secondly, the screening of core genes and pathways was solely conducted through bioinformatics analyses, including differential expression analysis, WGCNA, and LMM. *In vitro* experiments, such as NET induction experiments in GBC cell lines or core gene knockdown/overexpression experiments, were not performed to confirm the direct regulatory relationship between NETs and these genes/pathways. Similarly, *in vivo* experiments such as GBC xenograft models were not conducted to validate the pro-tumor effect of NETs. Hence, the conclusions drawn are essentially correlational, with a conspicuous lack of causal evidence. Lastly, this study did not delve into the association between NETs and GBC chemoresistance (for example, gemcitabine resistance) or treatment-related adverse reactions (such as myelosuppression). This oversight leaves the research hypothesis proposed in the introduction—that “NETs affect GBC treatment response”—partially unaddressed and also restricts the clinical application range of the results.

In light of the aforementioned limitations, future research should proceed in three key directions: Firstly, there is a need to increase the clinical sample size, ensuring the collection of GBC tissue samples that come with comprehensive clinicopathological information such as stage, treatment regimen, and prognosis. Subsequently, one should assess the expression levels of NET markers (e.g., cit-H3 and neutrophil elastase) and core genes (e.g., *ADAMTS1* and *GPX3*) through immunohistochemistry. This will aid in determining their association with patient prognosis, potentially identifying new prognostic markers. Secondly, functional experiments should be executed. For example, inducing NET formation or inhibiting NETs using PAD4 inhibitors in GBC cell lines (e.g., GBC-SD and NOZ) can shed light on alterations in core gene expression and pathway activity.<sup>58</sup> It is crucial to investigate the regulatory influence of NETs on GBC cell proliferation, invasion, and drug resistance. Clarifying the mechanism by which core genes facilitate the pro-tumor effect of NETs can be achieved through gene knockdown/overexpression experiments. Thirdly, there is an imperative to integrate clinical treatment requirements when constructing GBC chemoresistance models. Analyzing fluctuations in NET

expression during the resistance process and investigating the efficacy of NET-targeted therapy in conjunction with chemotherapy (e.g., gemcitabine + cisplatin) against drug-resistant cells can pave the way for innovative strategies to address GBC chemoresistance. Moreover, the core genes and pathways identified in this research offer avenues for subsequent mechanistic studies. Successfully translating these findings into clinical practice would align with the core objective of exploring novel molecular targets to enhance the effectiveness of conversion therapy for biliary tract malignancies, as delineated in the “Expert Consensus on Conversion Therapy of Biliary Tract Cancer”.<sup>5</sup> Such advancements would significantly contribute to refining GBC conversion therapy approaches, transitioning from “conventional systemic therapy” to “targeted therapy based on specific molecular markers,” given that GBC is a prominent subtype of biliary tract cancer.

## 5. Conclusion

This study aimed to address the existing research gap concerning NETs in GBC. It employed a bioinformatics analysis of public GEO datasets, implementing procedures such as batch effect correction, DEG screening, WGCNA-based module identification, and intersection with NET-related genes. This process led to the identification of 54 core genes and significant alterations in pathway activity, including the upregulation of cell cycle pathways and downregulation of inflammation pathways in GBC. The observed downregulation of *ADAMTS1* and *GPX3*, coupled with changes in pathway activity, suggests that NETs may contribute to GBC progression by disrupting the integrity of the ECM and balance of oxidative stress. This indicates the potential of a combined therapeutic strategy targeting NETs (e.g., with PAD4 inhibitors) and pathway-specific inhibitors (e.g., RB1 agonists) for GBC treatment. However, this study acknowledges limitations, such as a small sample size (25 patients), a lack of correlation with clinicopathological data, and reliance solely on bioinformatics without experimental validation. Future research should increase the clinical sample size, conduct functional experiments (such as NET induction or inhibition in GBC cell lines like GBC-SD and NOZ), and investigate the role of NETs in GBC chemoresistance. Overall, this study addresses the prevailing gap in NET-related GBC research, offering a theoretical foundation for the precise diagnosis and treatment of GBC. It aligns with clinical practice guidelines, thereby establishing a basis for subsequent translational studies.

## Acknowledgments

None.

## Funding

None.

## Conflict of interest

Meng-Yao Li is the Youth Editorial Board Member of this journal, but was not in any way involved in the editorial and peer-review process conducted for this paper, directly or indirectly. Separately, other authors declared that they have no known competing financial interests or personal relationships that could have influenced the work reported in this paper.

## Author contributions

*Conceptualization:* Shuai Ren, Meng-Yao Li

*Investigation:* Jintao Liang, Yalun Liang, Yimao Wu

*Methodology:* Jintao Liang, Yalun Liang, Yimao Wu

*Writing – original draft:* Jintao Liang, Yalun Liang, Yimao Wu

*Writing – review & editing:* Shuai Ren, Meng-Yao Li

## Ethical approval and consent to participate

Not applicable.

## Consent for publication

Not applicable.

## Availability of data

The datasets used and analyzed during the current study are available from the corresponding author on reasonable request. All analysis code, including batch correction parameters, differential expression analysis, WGCNA implementation, and downstream analyses, will be considered for deposition in the public repository GitHub upon publication and is also available from the corresponding author upon reasonable request.

## References

1. Roa JC, García P, Kapoor VK, Maithel SK, Javle M, Koshiol J. Gallbladder cancer. *Nat Rev Dis Primer*. 2022;8(1):69. doi: 10.1038/s41572-022-00398-y
2. Siegel RL, Kratzer TB, Giaquinto AN, Sung H, Jemal A. Cancer statistics, 2025. *CA Cancer J Clin*. 2025;75(1):10-45. doi: 10.3322/caac.21871
3. Kumar M, Kumar A, Srivastav A, Ghosh A, Kumar D. Genomic and molecular landscape of gallbladder cancer elucidating pathogenic mechanisms novel therapeutic targets and clinical implications. *Mutat Res*. 2025;830:111896. doi: 10.1016/j.mrfmmm.2024.111896
4. Zeng H, Zheng R, Sun K, *et al*. Cancer survival statistics in



- China 2019–2021: A multicenter, population-based study. *J Natl Cancer Cent.* 2024;4(3):203–213.  
doi: 10.1016/j.jncc.2024.06.005
5. Zhonghua Yixuehui Waike Xuehui Dandao Waike Xuezu, Zhongguo Yishizhe Xiehui Waike Yishizhe Xiehui Dandao Waike Zhuanjia Gongzuo Zu. [Expert consensus on the translational treatment of malignant biliary tumors (2025)]. *Zhonghua Waike Zazhi.* 2025;63(6):453–460.  
doi: 10.3760/cma.j.cn112139-20250310-00118
6. Xu B, Yin Y, Chang J, *et al.* Prognostic factors and treatment outcomes in gallbladder cancer patients undergoing curative surgery: A multicenter retrospective cohort study. *Curr Oncol Tor Ont.* 2025;32(6):328.  
doi: 10.3390/curroncol32060328
7. Shi G, Huang X, Ma L, *et al.* First-line tislelizumab and ociperlimab combined with gemcitabine and cisplatin in advanced biliary tract cancer (ZSAB-TOP): A multicenter, single-arm, phase 2 study. *Signal Transduct Target Ther.* 2025;10(1):260.  
doi: 10.1038/s41392-025-02356-y
8. Jayathilaka B, Mian F, Franchini F, Au-Yeung G, IJzerman M. Cancer and treatment specific incidence rates of immune-related adverse events induced by immune checkpoint inhibitors: A systematic review. *Br J Cancer.* 2025;132(1):51–57.  
doi: 10.1038/s41416-024-02887-1
9. Li MY, Zhang H, Li J, *et al.* Reshaping the future of cancer therapy: Taming toxicity and side effects. *Biomed Eng Commun.* 2026;5(2):11.  
doi: 10.53388/BMEC2026011
10. Filipczak N, Yalamarty SSK, Li X, *et al.* Neutrophil extracellular traps: Formation, pathological roles, and nanoparticle-based therapeutic targeting strategies. *J Control Release Off J Control Release Soc.* 2025;387:114220.  
doi: 10.1016/j.jconrel.2025.114220
11. Torres MDT, Cesaro A, De La Fuente-Nunez C. Peptides from non-immune proteins target infections through antimicrobial and immunomodulatory properties. *Trends Biotechnol.* 2025;43(1):184–205.  
doi: 10.1016/j.tibtech.2024.09.008
12. Demkow U. Neutrophil extracellular traps (NETs) in cancer invasion, evasion and metastasis. *Cancers.* 2021;13(17):4495.  
doi: 10.3390/cancers13174495
13. Guan X, Guan X, Zhao Z, Yan H. NETs: Important players in cancer progression and therapeutic resistance. *Exp Cell Res.* 2024;441(2):114191.  
doi: 10.1016/j.yexcr.2024.114191
14. Li MY, Zhang Q, Li J, Zengin G. Food and medicine homology in cancer treatment: Traditional thoughts collide with scientific evidence. *Food Med Homol.* 2025;2(3):9420120.  
doi: 10.26599/FMH.2025.9420120
15. Li JT, Gu A, Tang NN, Sun ZY, Zhang G, Li MY. Exploring anti-tumor potential of food and medicine homology substances: An in-silico evaluation of Citri Grandis Exocarpium against gallbladder cancer. *Food Med Homol.* 2026;3:9420084.  
doi: 10.26599/FMH.2026.9420084
16. Lee CJ, Jang TY, Jeon SE, *et al.* The dysadherin/MMP9 axis modifies the extracellular matrix to accelerate colorectal cancer progression. *Nat Commun.* 2024;15(1):10422.  
doi: 10.1038/s41467-024-54920-9
17. Cáceres-Calle D, Torre-Cea I, Marcos-Zazo L, *et al.* Integrins as key mediators of metastasis. *Int J Mol Sci.* 2025;26(3):904.  
doi: 10.3390/ijms26030904
18. Mempel TR, Lill JK, Altenburger LM. How chemokines organise the tumour microenvironment. *Nat Rev Cancer.* 2024;24(1):28–50.  
doi: 10.1038/s41568-023-00635-w
19. Narasaraaju T, Neeli I, Criswell SL, *et al.* Neutrophil activity and extracellular matrix degradation: Drivers of lung tissue destruction in fatal COVID-19 cases and implications for long COVID. *Biomolecules.* 2024;14(2):236.  
doi: 10.3390/biom14020236
20. Zhang Z, Niu R, Zhao L, Wang Y, Liu G. Mechanisms of neutrophil extracellular trap formation and regulation in cancers. *Int J Mol Sci.* 2023;24(12):10265.  
doi: 10.3390/ijms241210265
21. Kwon HJ, Lee GS, Moon JH, Jung J. Activation of G protein-coupled estrogen receptor induces p53 and ADAMTS1 to inhibit tumor growth and suppress liver cancer metastasis. *Cancers.* 2025;17(16):2623.  
doi: 10.3390/cancers17162623
22. Melia E, Parsons JL. The potential for targeting G2/M cell cycle checkpoint kinases in enhancing the efficacy of radiotherapy. *Cancers.* 2024;16(17):3016.  
doi: 10.3390/cancers16173016
23. Schoen J, Euler M, Schauer C, *et al.* Neutrophils' extracellular trap mechanisms: From physiology to pathology. *Int J Mol Sci.* 2022;23(21):12855.  
doi: 10.3390/ijms232112855
24. Zhang C, Wu D, Dong B, *et al.* The scaffold of neutrophil extracellular traps promotes CCA progression and modulates angiogenesis via ITGAV/NFκB. *Cell Commun Signal.* 2024;22(1):103.  
doi: 10.1186/s12964-024-01500-5

25. Li N, Yin C, Tao J. Neutrophil extracellular traps in tumor metastasis: Mechanisms, and therapeutic implications. *Discov Oncol.* 2025;16(1):1631.  
doi: 10.1007/s12672-025-03451-w
26. Yamaguchi H, Miyazaki M. Heterocellular adhesion in cancer invasion and metastasis: Interactions between cancer cells and cancer-associated fibroblasts. *Cancers.* 2024;16(9):1636.  
doi: 10.3390/cancers16091636
27. Kurtyka M, Wessely F, Bau S, *et al.* The solute carrier SLC7A1 may act as a protein transporter at the blood-brain barrier. *Eur J Cell Biol.* 2024;103(2):151406.  
doi: 10.1016/j.ejcb.2024.151406
28. Rao D, Li J, Zhang M, *et al.* Multi-model analysis of gallbladder cancer reveals the role of oxLDL-absorbing neutrophils in promoting liver invasion. *Exp Hematol Oncol.* 2024;13(1):58.  
doi: 10.1186/s40164-024-00521-7
29. Azzouz D, Palaniyar N. How do ROS induce NETosis? Oxidative DNA damage, DNA repair, and chromatin decondensation. *Biomolecules.* 2024;14(10):1307.  
doi: 10.3390/biom14101307
30. Tatarova Z. Using the tumour microenvironment to improve therapy efficacy. *Nat Rev Cancer.* 2024;24(7):444.  
doi: 10.1038/s41568-024-00693-8
31. Liu F, Wu Q, Dong Z, Liu K. Integrins in cancer: Emerging mechanisms and therapeutic opportunities. *Pharmacol Ther.* 2023;247:108458.  
doi: 10.1016/j.pharmthera.2023.108458
32. Shang B, Cui H, Xie R, *et al.* Neutrophil extracellular traps primed intercellular communication in cancer progression as a promising therapeutic target. *Biomark Res.* 2023;11(1):24.  
doi: 10.1186/s40364-023-00463-y
33. Adrover JM, McDowell SAC, He XY, Quail DF, Egeblad M. NETworking with cancer: The bidirectional interplay between cancer and neutrophil extracellular traps. *Cancer Cell.* 2023;41(3):505-526.  
doi: 10.1016/j.ccell.2023.02.001
34. Chen Y, Hu H, Tan S, *et al.* The role of neutrophil extracellular traps in cancer progression, metastasis and therapy. *Exp Hematol Oncol.* 2022;11(1):99.  
doi: 10.1186/s40164-022-00345-3
35. Wu Y, Sun R, Ren S, Zengin G, Li M. Neuronal reshaping of the tumor microenvironment in tumorigenesis and metastasis: Bench to clinic. *Med Adv.* 2025;3(4):364-371.  
doi: 10.1002/med4.70044
36. Hu J. Stress-induced metastasis: The NET effect. *Cancer Cell.* 2024;42(3):335-337.  
doi: 10.1016/j.ccell.2024.02.005
37. Gao F, Peng H, Gou R, Zhou Y, Ren S, Li F. Exploring neutrophil extracellular traps: mechanisms of immune regulation and future therapeutic potential. *Exp Hematol Oncol.* 2025;14(1):80.  
doi: 10.1186/s40164-025-00670-3
38. Tan IA, Ricciardelli C, Russell DL. The metalloproteinase ADAMTS1: A comprehensive review of its role in tumorigenic and metastatic pathways. *Int J Cancer.* 2013;133(10):2263-2276.  
doi: 10.1002/ijc.28127
39. Vilaça-Faria H, Noro J, Reis RL, Pirraco RP. Extracellular matrix-derived materials for tissue engineering and regenerative medicine: A journey from isolation to characterization and application. *Bioact Mater.* 2024;34:494-519.  
doi: 10.1016/j.bioactmat.2024.01.004
40. Zhang N, Liao H, Lin Z, Tang Q. Insights into the role of glutathione peroxidase 3 in non-neoplastic diseases. *Biomolecules.* 2024;14(6):689.  
doi: 10.3390/biom14060689
41. Azzouz D, Palaniyar N. How do ROS induce NETosis? Oxidative DNA damage, DNA repair, and chromatin decondensation. *Biomolecules.* 2024;14(10):1307.  
doi: 10.3390/biom14101307
42. Chen A, Huang H, Fang S, Hang Q. ROS: A “booster” for chronic inflammation and tumor metastasis. *Biochim Biophys Acta BBA - Rev Cancer.* 2024;1879(6):189175.  
doi: 10.1016/j.bbcan.2024.189175
43. Zhao Y, Ye X, Xiong Z, *et al.* Cancer metabolism: the role of ROS in DNA damage and induction of apoptosis in cancer cells. *Metabolites.* 2023;13(7):796.  
doi: 10.3390/metabo13070796
44. Wang Y, Liu F, Chen L, *et al.* Neutrophil extracellular traps (NETs) promote non-small cell lung cancer metastasis by suppressing lncRNA MIR503HG to activate the NF-κB/NLRP3 inflammasome pathway. *Front Immunol.* 2022;13:867516.  
doi: 10.3389/fimmu.2022.867516
45. Zhang A, Zou X, Yang S, Yang H, Ma Z, Li J. Effect of NETs/COX-2 pathway on immune microenvironment and metastasis in gastric cancer. *Front Immunol.* 2023;14:1177604.  
doi: 10.3389/fimmu.2023.1177604
46. Bertoli C, Skotheim JM, De Bruin RAM. Control of cell cycle transcription during G1 and S phases. *Nat Rev Mol Cell Biol.* 2013;14(8):518-528.

doi: 10.1038/nrm3629

47. Jung Y, Kraikivski P, Shafiekhani S, Terhune SS, Dash RK. Crosstalk between Plk1, p53, cell cycle, and G2/M DNA damage checkpoint regulation in cancer: Computational modeling and analysis. *NPJ Syst Biol Appl*. 2021;7(1):46.

doi: 10.1038/s41540-021-00203-8

48. Oshi M, Patel A, Le L, *et al*. G2M checkpoint pathway alone is associated with drug response and survival among cell proliferation-related pathways in pancreatic cancer. *Am J Cancer Res*. 2021;11(6):3070-3084.

49. Chida K, Oshi M, Roy AM, *et al*. E2F target score is associated with cell proliferation and survival of patients with hepatocellular carcinoma. *Surgery*. 2023;174(2):307-314.

doi: 10.1016/j.surg.2023.04.030

50. Guan X, Guan X, Zhao Z, Yan H. NETs: Important players in cancer progression and therapeutic resistance. *Exp Cell Res*. 2024;441(2):114191.

doi: 10.1016/j.yexcr.2024.114191

51. Wang Z, Liu Z, Lv M, Luan Z, Li T, Hu J. Novel histone modifications and liver cancer: Emerging frontiers in epigenetic regulation. *Clin Epigenetics*. 2025;17(1):30.

doi: 10.1186/s13148-025-01838-8

52. Li J, Gu A, Tang N, Zengin G, Li M, Liu Y. Patient-derived xenograft models in pan-cancer: From bench to clinic. *Interdiscip Med*. 2025;3(5):e20250016.

doi: 10.1002/INMD.20250016

53. Mao H, Zhao X, Sun SC. NF- $\kappa$ B in inflammation and cancer. *Cell Mol Immunol*. 2025;22(8):811-839.

doi: 10.1038/s41423-025-01310-w

54. Jeon MT, Cogill SA, Kim KS, *et al*. TNF- $\alpha$ -NF- $\kappa$ B activation through pathological  $\alpha$ -synuclein disrupts the BBB and exacerbates axonopathy. *Cell Rep*. 2025;44(7):116001.

doi: 10.1016/j.celrep.2025.116001

55. Manoj H, Gomes SM, Thimmappa PY, Nagareddy PR, Jamora C, Joshi MB. Cytokine signalling in formation of neutrophil extracellular traps: Implications for health and diseases. *Cytokine Growth Factor Rev*. 2025;81:27-39.

doi: 10.1016/j.cytogfr.2024.12.001

56. Gao F, Peng H, Gou R, Zhou Y, Ren S, Li F. Exploring neutrophil extracellular traps: Mechanisms of immune regulation and future therapeutic potential. *Exp Hematol Oncol*. 2025;14(1):80.

doi: 10.1186/s40164-025-00670-3

57. Singhal K, Malya, Verma H, Bharti B. Modulation of NF- $\kappa$ B pathway in cancer therapy by sodium butyrate and isoproterenol. *Mol Biol Rep*. 2025;52(1):938.

doi: 10.1007/s11033-025-11047-4

58. Wu G, Fan X, Cheng L, *et al*. Metabolism-driven posttranslational modifications and immune regulation: Emerging targets for immunotherapy. *Sci Adv*. 2025;11(37):eadx6489.

doi: 10.1126/sciadv.adx6489

59. Li MY, Gu A, Li J, *et al*. Exploring food and medicine homology: Potential implications for cancer treatment innovations. *Acta Mater Med*. 2025;4(2):200-206.

doi: 10.15212/AMM-2025-0003

Appendix

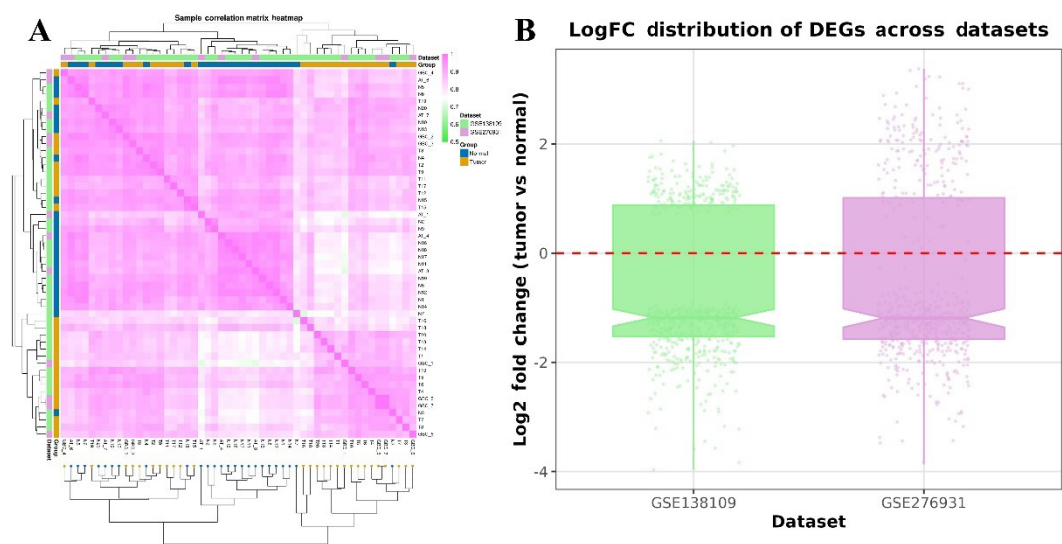


**Figure A1.** (A) Heatmap of the top 200 differentially expressed genes (DEGs; ranked by log Fold Change). (B) Heatmap showing expression patterns of the top 200 DEGs. Samples labeled by dataset (GSE138109: green, GSE276931: purple).

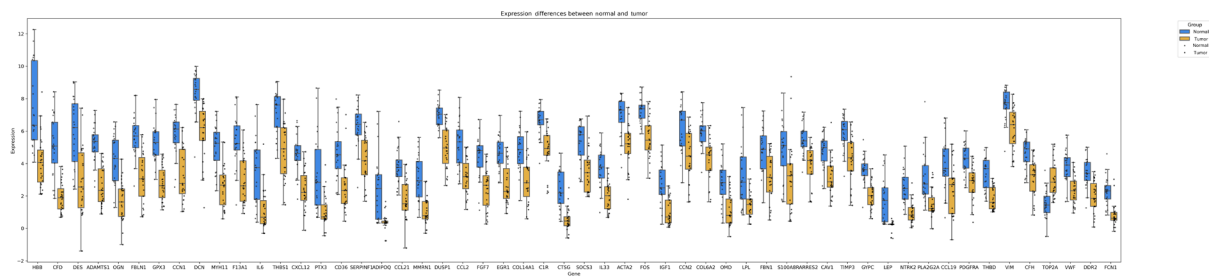


**Figure A2.** Boxplot illustrating statistical differences in expression levels of 54 core genes between tumor and normal tissues